Scientific Research Report

Mechanical Properties and Microstructure of 3D-Printed Zirconia Based on Sintering Placement Orientation

Qi Jia [a], Seo-Hyun Kim [a,b], Yuchuan Xu [c], Chen Ma [c], Kwang-Mahn Kim [a], Heng Bo Jiang [c*], Jae-Sung Kwon [a,b*]

[a] Department and Research Institute of Dental Biomaterials and Bioengineering, Yonsei University College of Dentistry, Seoul 03722, Republic of Korea
[b] BK21 FOUR Project, Yonsei University College of Dentistry, Seoul 03722, Republic of Korea
[c] The CONVERSATIONALIST club & Department of Dental Digitalization, School of Stomatology, Shandong First Medical University, Jinan, Shandong 250117, China

ARTICLE INFO

Article history:
Received 21 May 2025
Received in revised form
23 September 2025
Accepted 25 September 2025
Available online 24 October 2025

Keywords:
ZrO_2
3D-printing
Sintering
Orientation
Anisotropy
Microstructure

ABSTRACT

Objective: Sintering is a critical step in fabricating 3D-printed zirconia (3Dp/ZrO_2) restorations and is significantly influenced by gravity. Additionally, the layer-by-layer structure of 3Dp/ZrO_2 introduces anisotropy. Therefore, this study aims to investigate the influence of sintering placement orientation on the mechanical properties and microstructure of 3Dp/ZrO_2.

Materials and Methods: A digital light processing-type 3D printer and ZrO_2 slurry were used to fabricate green bodies, after which one-step sintering was used to create sintered 3Dp/ZrO_2 products. Group-A: Sintered with the printing layer orientation parallel to the horizontal plane. Group-B: Sintered with the printing layer orientation perpendicular to horizontal plane, with the short axis aligned vertically. Group-C: Sintered with the printing layer orientation perpendicular to horizontal plane, with the long axis aligned vertically. Shrinkage ratio, bulk density, three-point and biaxial flexure tests, scanning electron microscopy with energy dispersive spectrometry, X-ray diffraction, and micro-computed tomography were used to determine the physical, mechanical, and microstructural properties of the sintered 3Dp/ZrO_2 specimens.

Results: Group-B (558.28 ± 102.01 MPa) and Group-C (423.47 ± 38.46 MPa) showed a significantly lower flexure strength than Group-A (789.25 ± 57.10 MPa). More grain boundary defects and microdefects were observed in Group-B and Group-C. Different sintering placement orientations did not cause significant differences in shrinkage ratio, density, phase, or grain size.

Conclusions: The sintering placement orientation of 3Dp/ZrO_2 influenced its mechanical properties and microstructure. Sintering with the printing layer orientation parallel to horizontal plane showed superior mechanical properties. In contrast, the perpendicular orientation showed compromised performance, likely due to loose grain boundaries and internal microdefects observed within 3Dp/ZrO_2.

Clinical Significance: This study provides practical guidance for dental professionals by demonstrating how sintering placement orientation affects the microstructure of 3Dp/ZrO_2. Considering placement orientation during sintering process can help reduce defects and improve the mechanical properties of zirconia-based restorations for better clinical outcomes.

* *Corresponding authors*. The CONVERSATIONALIST club & Department of Dental Digitalization, School of Stomatology, Shandong First Medical University, Jinan 250117, Shandong, China; BK21 FOUR Project, Yonsei University College of Dentistry, Seoul 03722, Republic of Korea.
E-mail addresses: hbjiang@sdfmu.edu.cn (H.B. Jiang), jkwon@yuhs.ac (J.-S. Kwon).

Qi Jia: http://orcid.org/0000-0002-6355-8656
Chen Ma: http://orcid.org/0009-0000-8398-5519
Kwang-Mahn Kim: http://orcid.org/0000-0002-5235-0294
Heng Bo Jiang: http://orcid.org/0000-0002-2514-2633
Jae-Sung Kwon: http://orcid.org/0000-0001-9803-7730

https://doi.org/10.1016/j.identj.2025.103972

Introduction

Zirconia (ZrO_2) has gained significant attention in dentistry because of its outstanding mechanical properties, corrosion resistance, and biocompatibility.[1] Currently, the most commonly used technique for processing ZrO_2 is milling. However, the post-processing methods associated with milling can compromise the mechanical properties of ZrO_2 and do not produce complex, customized geometries. The emergence of 3D-printing technology offers a solution to these problems, enabling the creation of intricate geometric designs with high precision, material efficiency, speed, and personalisation.[2] These advantages have made 3D printing a popular choice in dentistry for applications such as crowns, scaffolds, surgical guides, and denture bases.[3] As research on zirconia-based 3D printing advances, techniques such as stereolithography, digital light processing (DLP), inkjet printing, material extrusion robocasting, and direct ink writing have become more prominent.[4] In particular, DLP-type 3D printers have drawn significant attention owing to their exceptional efficiency and accuracy, making them well-suited for dental applications.[5,6]

DLP technology enables the production of highly precise ZrO_2 dental restorations by curing a slurry composed of ZrO_2 powder and photopolymer resin. It builds the green body layer by layer, followed by debinding and sintering to produce dense 3D-printed ZrO_2 (3Dp/ZrO_2). According to previous studies, DLP-type 3D printers have been used to successfully print dental crowns.[7,8] However, although the flexural strength of 3Dp/ZrO_2 surpasses the minimum requirements of the ISO 6872 standards for clinical use, the mechanical properties of 3Dp/ZrO_2 are typically lower than those of milling groups.[4] According to a study[9], although the mean values of the biaxial flexural strength of 3Dp/ZrO_2 are similar to those of milled ZrO_2, the standard deviations of 3Dp/ZrO_2 are greater than those of conventionally milled ZrO_2. The mechanical properties of 3Dp/ZrO_2 are affected by various factors, including printing technique,[10-12] exposure time,[13] slurry composition,[14] cleaning solution,[15] sintering rate,[16] and surface treatment.[17] Therefore, a clear demonstration of improvements to the mechanical properties and stability of 3Dp/ZrO_2 is still required.

The layered structure of 3Dp/ZrO_2 is its most important characteristic. The manufacturing process and microstructure of 3Dp/ZrO_2 differ completely from those of conventional technologies, which brings about challenges in controlling its material properties. A study reported that flexural strength of 3Dp/ZrO_2 was significantly higher when the load orientation was parallel to the printing layer orientation than when it was perpendicular.[17] And another study reported that the Weibull characteristic strength was 920.22 MPa when the shorter-axis was vertical to ground in printing process, while it was 219.59 MPa when the longer-axis was vertical to ground.[18] Also, fatigue test confirmed that perpendicular printed specimens generated lower survival probabilities than parallel.[19] Such studies suggested that the 3Dp/ZrO_2 was not anisotropy. In sintering stage, the shrinkage in the Z-axis is considerably higher than that in the X- and Y-axes, even double as reported in one study.[20]

The anisotropy of 3Dp/ZrO_2 is inseparable from its microstructure. A previous study developed a sintering model for the numerical prediction of sintering process, with a lower viscosity in the Z-axis direction, further justifying the greater shrinkage in that direction.[21] They found more porous structures in the interlayer region, demonstrating that the origin of the shrinkage was a result of the structured porous microstructure. It was demonstrated the formation of interconnected channels during the sintering of ceramics by measuring the sintered products at different temperature and analysing their microstructure.[22] And the study suggested that by ensuring the smooth discharge of the melted binder and gaseous decomposition products during the low-temperature debinding stage, gas expansion leading to cracks could be avoided by reasonable temperature control during the high-temperature debinding stage. Driving force[23], built-in stress[24], and decomposition force[24] have also been found to affect the final grain boundaries and defect generation. It was found that during sintering, gravity causes distortions and deflections in the center of samples with higher aspect ratios and overhang configurations,[25] indicating that although the layered structure disappears after sintering, particle rearrangement during sintering could cause significant variations in the shape and properties of the product.

During the debinding and sintering stages, the particle rearrangement and gas escape processing may vary depending on whether the printing layer orientation is parallel or perpendicular to gravity. However, none of the studies have reported how the specimen placement orientation was controlled during the debinding and sintering processes, although the anisotropy of 3Dp/ZrO_2 has been extensively investigated. Also, supports inside the restorations have to be avoided, as they are difficult to remove and polish. This constraint limits the choice of printing orientation and necessitates a specific orientation that minimizes internal supports. However, some restorations without supports cannot be debinded and sintered with the printing layer orientation parallel to the horizontal plane because of their specific shapes, such as the central incisor, lateral incisor, and canine.

In this study, we evaluated the effect of different sintering placement orientations on the mechanical properties and microstructure of 3Dp/ZrO_2. The null hypothesis of this study was that the sintering placement orientation does not influence the characterisation, mechanical properties, or microstructure of 3Dp/ZrO_2. The shrinkage ratio, density and X-ray diffraction (XRD) analysis were conducted to characterise 3Dp/ZrO_2. Three-point and biaxial flexure tests were performed to determine the mechanical properties. Scanning electron microscopy (SEM) with energy dispersive spectrometry (EDS) and micro-computed tomography (micro-CT) were used to investigate the microstructural variations induced by different sintering placement orientations. Finally, by systematically analysing the results, we sought to develop guidelines for optimising the sintering placement of 3Dp/ZrO_2 to improve its application especially in dentistry.

Materials and methods

Specimens' fabrication

A ZrO_2 slurry (INNI-CERA, AON Co., Ltd.) was used as the raw material in this study. All specimens for each experiment were designed using CAD software (3D Builder, Microsoft) and exported as STL files. The STL models were enlarged according to the manufacturer's instructions (X-axis: 128.29%, Y-axis: 129.11%, Z-axis: 133.88%). The models were then sliced using sliced software (ZiproS, AON Co., Ltd.), with the layer thickness set to 0.05 mm with a printing speed of 6 mm/h. A DLP-type 3D printer (ZIPRO Dental, AON Co., Ltd., Korea) with lateral resolution 40 μm was used to fabricate the specimens. (Figure 1A) The light source was a 405 nm-wavelength ultraviolet LED. After printing, the supports were removed, and isopropyl alcohol was used to remove the remaining slurry from the specimen surface. Bar specimens with dimensions of $4 \times 4 \times 10$ mm^3 were used for the characterisations analysis and microstructure observation. In accordance with ISO 6872:2015, $3 \times 4 \times 25$ mm^3 bar specimens were used for the three-point flexure tests, while 14.2 mm-diameter and 1.2 mm-thick disc specimens were used for the biaxial flexure tests.

Debinding and sintering

We used a conventional box-type electric furnace (CERAFUR, AON, Korea) to improve the universality and reproducibility of the results. The furnace chamber is cylindrical (heating zone: 105 mm diameter × 100 mm height). The furnace type is radiation-based resistance heating and heating is provided by molybdenum disilicide resistive heating elements, exposed on the side walls.

To investigate the influence of sintering placement orientation on the mechanical properties and microstructure of 3DP/ZrO_2, specimens were debinded and sintered in three orientations, as illustrated in Figure 1B. Group-A: The specimens were placed with the printing layer orientation parallel to the horizontal plane. Group-B: The specimens were placed with the printing layer orientation perpendicular to horizontal plane, with the specimen's short axis aligned vertically (parallel to gravity). Group-C: The specimens were placed with the printing layer orientation perpendicular to horizontal plane, with the specimen's long axis aligned vertically (parallel to gravity). And since there are only two possible sintering placement orientations of the disc, only two groups, Group-A and Group-B, were included in the biaxial flexure test. A specific one-step sintering procedure (including debinding and sintering process) was used in this study (Figure 2). After sintering, specimens were progressively polished from grade #400 to grade #1000 using diamond grinding discs and finally polished with colloidal silica polishing suspension with a nominal abrasive size of 0.06 μm (MasterMet, BUEHLER, USA). The specimens were then rinsed with ethyl alcohol and blow-dried.

Shrinkage ratio, density and phase compositions

For shrinkage ratios, the X, Y, and Z lengths were measured before (L_0) and after (L) sintering. The shrinkage ratio of 3Dp/ZrO_2 specimens was calculated using Eq. (1). (N = 6)

$$\textit{Shrinkage ratio} = \frac{L_0 - L}{L_0} \times 100\%. \quad (1)$$

For density test, the 3Dp/ZrO_2 specimens were firstly dried for 3 h in a furnace at 110°C before measuring the dry mass (m_1). Subsequently, the specimens were placed in distilled water and boiled for 3 h. The soaked specimens were maintained in 20°C environment. The masses of the immersed test specimens (m_2) and the mass of the soaked specimens (m_3) were measured. The density of each specimen was calculated using Eq. (2). (N = 6)

$$\rho = \frac{m_1}{m_3 - m_2} \times \rho_l, \quad (2)$$

where $\rho_l = 998.2$ kg/m^3.

XRD analyses (Ultima IV, Rigaku, Japan) of the printing and lateral surfaces of all groups were performed. The specimens

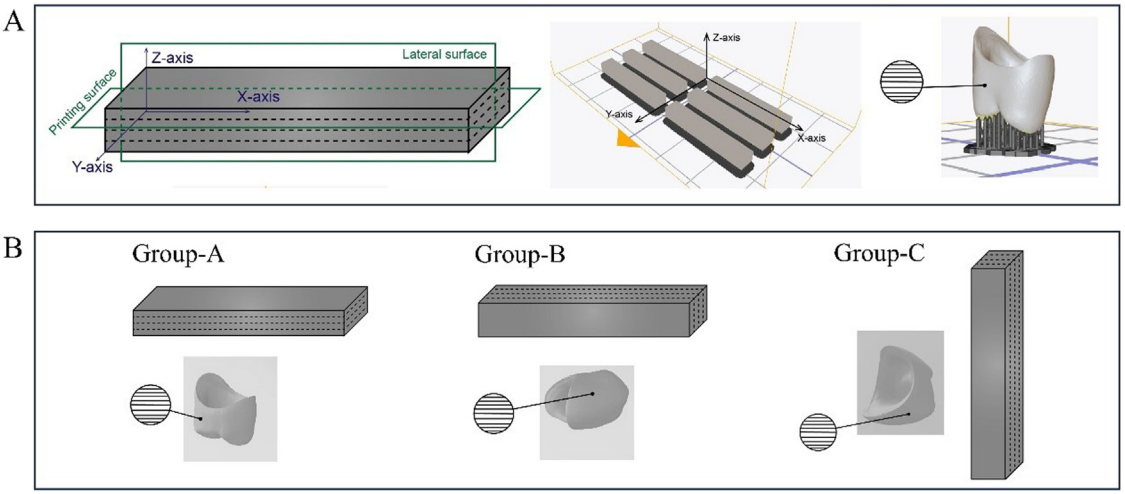

Fig. 1 – (A) Illustration of the printing layer orientation. Lateral surface indicates the center surface in Y-axis and printing surface indicates the center surface of Z-axis. (B) Illustration of the sintering placement orientation.

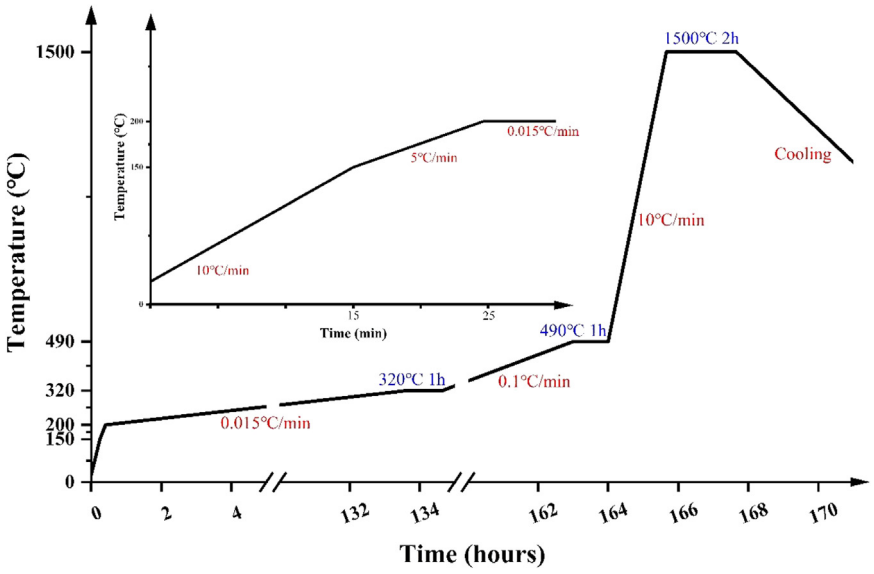

Fig. 2 – Debinding and sintering curve of 3Dp/ZrO_2.

were scanned using Cu/Kα (40 kV, 40 mA) irradiation from 20° to 90° with a step size of 0.02° for 3 s.

Three-point flexure test

All 3Dp/ZrO_2 specimens were loaded to fracture using a Universal Test Machine (UTM, INSTRON) with a crosshead speed of 1 mm/min and 20 mm spacing between the support roller centers. The flexural strength and modulus of each specimen were calculated using Eqs. (3) and (4). (N = 6)

$$Flexural\ Strength = \frac{3Fl}{2wh^2}, \tag{3}$$

$$Flexural\ Modulus = \frac{Fl^3}{4wh^3d}, \tag{4}$$

where F is the breaking load (N), l is the test span (20 mm center-to-center between the support roller), w is the width of the specimen (mm), h is the thickness of the specimen (mm), and d is the deflection at F (mm).

Biaxial flexure test

All 3Dp/ZrO_2 specimens were loaded to fracture using a UTM with a crosshead speed of 1 mm/min. The radius of the three support balls was 6 mm, and that of the load rod was 0.6 mm. The biaxial strength of each specimen was calculated using Eq. (5). (N = 6)

$$Biaxial\ Strength\ \sigma = -\frac{0.2387P(K1 - K2)}{b^2}, \tag{5}$$

where P is the total load causing fracture (N), K1 = (1+v)ln $(r2/r3)^2$+[(1-v)/2]$(r2/r3)^2$, and K2 = (1+v)[1+ln$(r1/r3)^2$]+(1-v) $(r1/r3)^2$. ν is Poisson's ratio (0.25), r1 is the support circle radius (6 mm), r2 is the loaded area (0.6 mm), r3 is the specimen radius (7.1 mm), and b is the specimen thickness at the fracture origin (mm).

Microstructure analysis

The green bodies were gently ground using diamond discs from grade #400 to grade #1000 to smooth the lateral surface for observation, and the layered structure was confirmed by EDS elemental mapping of the lateral surface (as shown in Figure 1A). After sintering, we also analysed the elemental distribution of the lateral surface of sintered 3Dp/ZrO_2 specimens. Also, the SEM images of the printing and lateral surfaces (as shown in Figure 1A) of the sintered 3Dp/ZrO_2 specimens were obtained for microstructure analysis. Grain sizes were measured for each surface using ImageJ software (v.1.54, USA) and each group contained no fewer than 750 measured grains. Before SEM operation, the sintered 3Dp/ZrO_2 specimens were sintered in a furnace at 1200 °C for 2 hours before coating as thermal etching treatment. And Pt/Au coating time was set to 200 seconds.

A representative 3Dp/ZrO_2 Specimen from each group were scanned using micro-CT (SkyScan 1173). The micro-CT scanner had a 130 kV voltage, 60 μA current, 360° rotation scan mode, and 7.14 μm pixel size. Both the 2D slices and 3D files were analysed by the micro-CT analysis program (CTAn-CTVol 1.10).

Statistical analysis

One-way analysis of variance (ANOVA, Origin2022, OriginLab, USA) was used for all tests. Tukey's post-hoc analysis was performed. The confidence level was set at 95%. And post-hoc power analysis was performed to confirm reliability of the results (α = 0.05).

Results

Shrinkage ratio, density and phase compositions

Figure 3A shows the shrinkage ratio of 3Dp/ZrO_2. No significant differences between Group-A, Group-B and Group-C can

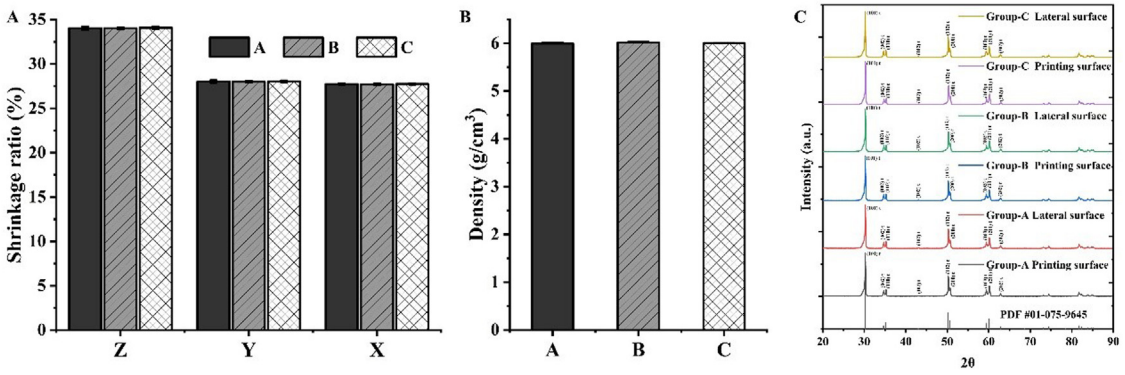

Fig. 3 – (A) Shrinkage ratios of Group-A, Group-B, and Group-C along the X-, Y-, and X-axis; (B) Densities of Group-A, Group-B, and Group-C. (C) XRD analyses of the printing and lateral surfaces of Group-A, Group-B, and Group-C with reference PDF 01-075-9645. t: tetragonal phase.

be observed on the same axis. The shrinkage ratios (%) of Group-A on the X-, Y-, and Z-axes were 27.72 ± 0.07, 28.01 ± 0.14, and 34.03 ± 0.18, respectively. The shrinkage ratios (%) of Group-B on the X-, Y-, and Z-axes were 27.69 ± 0.11, 27.99 ± 0.10, and 34.03 ± 0.12, respectively. The shrinkage ratios (%) of Group-C on the X-, Y-, and Z-axes were 27.74 ± 0.07, 28.02 ± 0.11, and 34.08 ± 0.14, respectively. These values are similar to those provided by the manufacturer.

Figure 3B shows the bulk density of sintered 3Dp/ZrO_2. The densities of Group-A, Group-B, and Group-C were 6.00 ± 0.03, 6.02 ± 0.01, and 6.00 ± 0.01 g/cm^3, respectively. The different sintering placement orientations are thus not expected to lead to obvious differences in density.

The XRD intensity patterns for all groups are presented in Figure 3C. Group-A, Group-B, and Group-C only exhibited the tetragonal phase compositions, indicating that the different sintering placement orientations did not result in phase composition changes.

Three-point and biaxial flexural test

Figure 4A-C shows the 3-point flexure results for sintered 3Dp/ZrO_2. The flexural strength of the 3 groups differed significantly ($p < .001$) with 100 % power to detect the difference: 789.25 ± 57.10 MPa for Group-A, 558.28 ± 102.01 MPa for Group-B, and 423.47 ± 38.46 MPa for Group-C. The flexural modulus of Group-C (13.48 ± 1.56 GPa) was lower than and Group-B (14.18 ± 1.00 GPa) those of Group-A (14.52 ± 2.98 GPa). This indicated that a sintering with the printing layer orientation parallel to the horizontal plane is preferable in terms of three-point flexure.

Figure 4D the biaxial flexural tests. The biaxial strength of Group-B (952.40 ± 199.71 MPa) was lower than that of Group-A (1001.66 ± 199.37 MPa). Although there was no significant difference in the biaxial flexure tests, the strength of Group-B was lower than that of Group-A.

Microstructure

As shown in Figure 5A, the green body exhibited a layered structure. Less Zr can be observed in the bonding region between the layers, indicating that less ZrO_2 was present. Further, a fuzzy transitional boundary can be observed at the top of the layer and a clear, straight boundary at the bottom of the layer. The anisotropy of green body existed not only in the entire sample but also within the single layer. However, this phenomenon was observed to disappear after sintering (Figure 5B). Both the SEM images and EDS analysis revealed a uniform surface for 3Dp/ZrO_2.

The grain size distribution (Figure 6A) for both the printed and lateral surfaces of 3Dp/ZrO_2 exhibited similar results for all groups. More than 50% of the grain sizes were between 0.3 and 0.6 μm. As indicated by the yellow arrows in Figure 6B, the grain boundaries in Group-B and Group-C were not as tight as those in Group-A. Moreover, as indicated by the blue circles, more lacuna microdefects can be observed in Group-B and Group-C than in Group-A.

Figure 6C shows no obvious defects in the 2D slices and 3D files for Group-A, Group-B, and Group-C, as obtained via micro-CT. This proves that the different sintering placement orientations did not lead to obvious defects.

Discussion

The purpose of this study was to evaluate the effect of different sintering placement orientations on the mechanical properties and microstructure of 3Dp/ZrO_2. The shrinkage ratio, density, flexural strength, element distribution, grain size distribution, grain boundaries, microdefects, phase compositions, and micro-CT results were analysed. According to the three-point and biaxial flexure test results, the perpendicular sintering placement orientation (Group-B and Group-C) exhibited a significantly lower strength than the parallel sintering placement orientation (Group-A), revealing that sintering placement orientation influences flexural strength. Note that sintering placement orientation affected the grain boundaries, microdefects, and even cracks. Therefore, the hypothesis that sintering placement orientation does not influence the mechanical properties and microstructure is rejected.

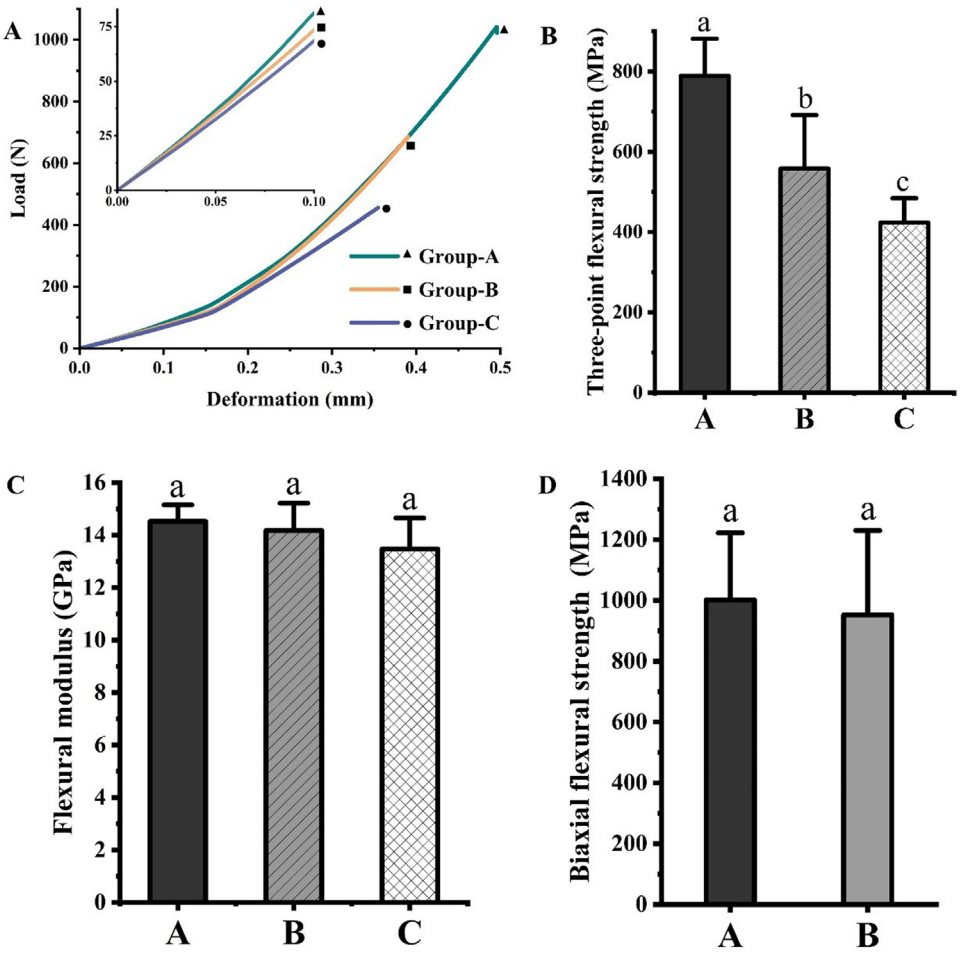

Fig. 4 – (A-C) Three-point flexure results of Group-A, Group-B, and Group-C. (A) Load–deformation curve. (B) Three-point flexural strength. (C) Flexural modulus. (D) Biaxial flexural strength.

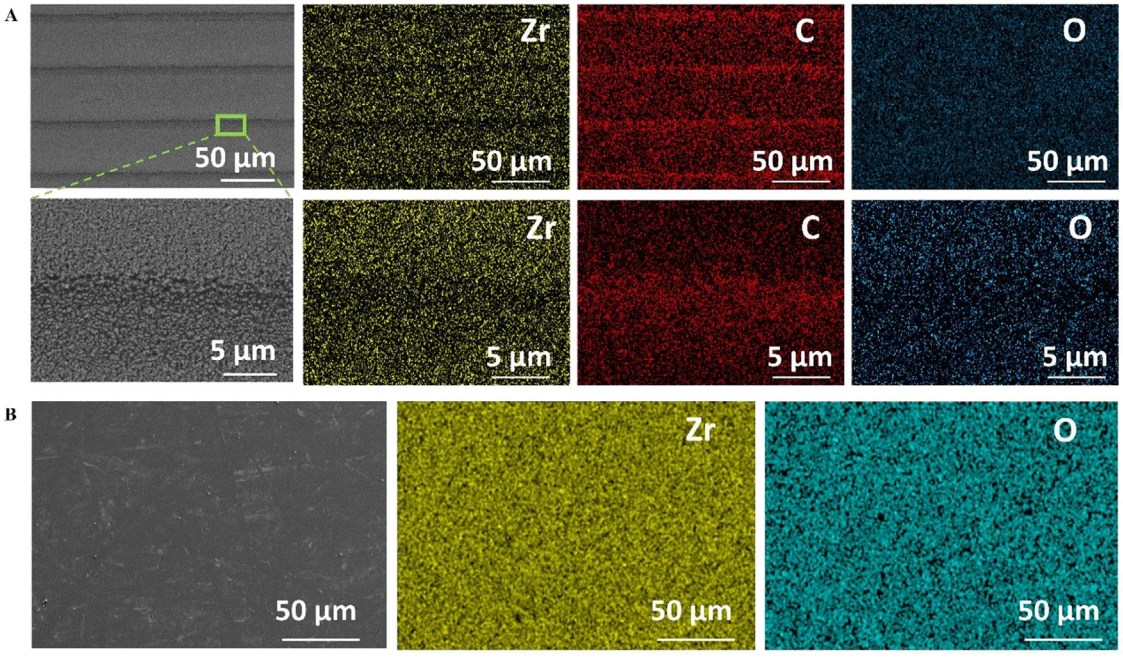

Fig. 5 – (A) SEM and EDS mapping images of the lateral surface of the green body. (B) SEM and EDS mapping of the lateral surface of 3Dp/ZrO_2. Yellow, red, and blue colors represent Zr, C, and O, respectively.

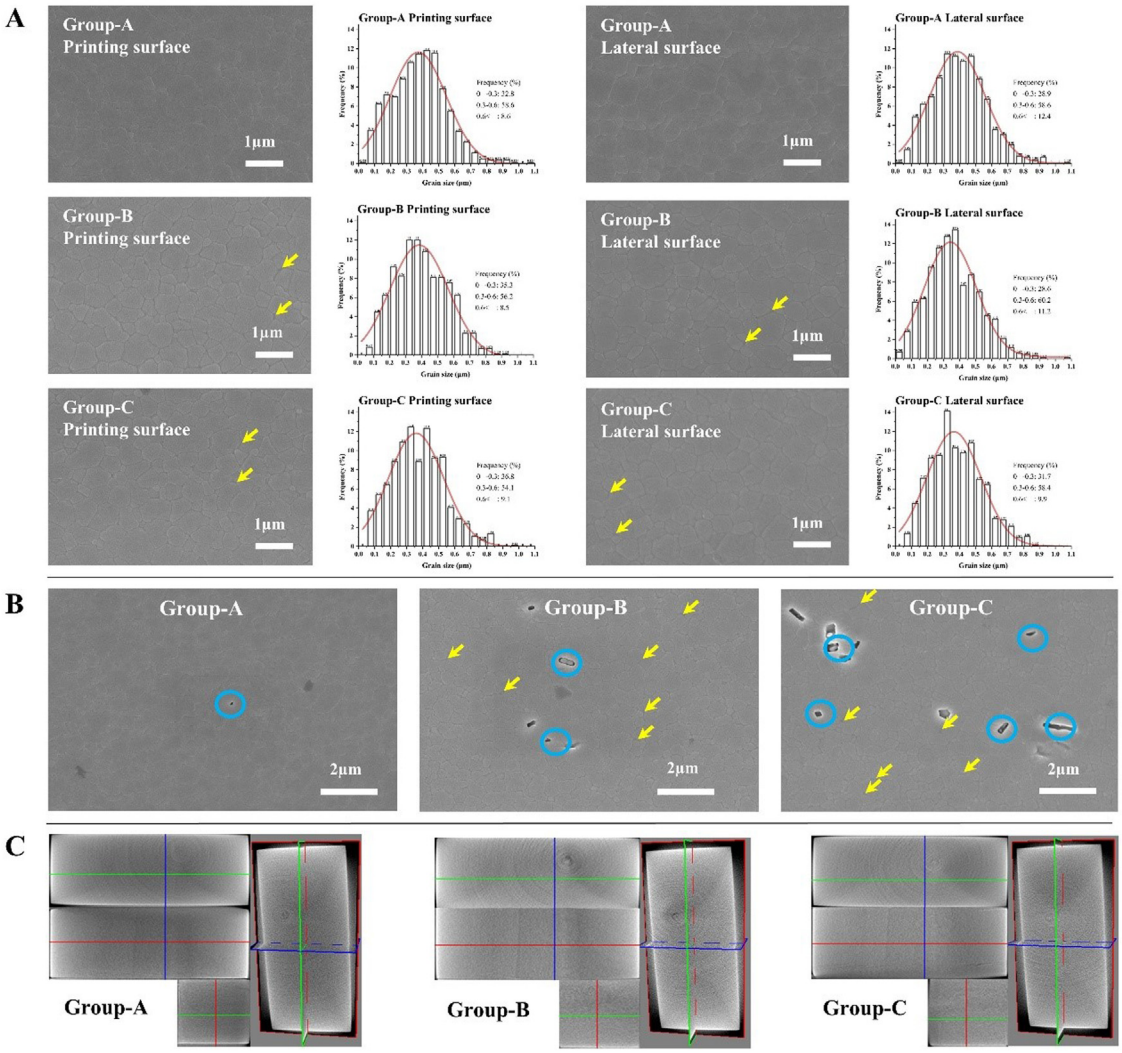

Fig. 6 – Microstructure analysis of sintered 3Dp/ZrO_2. (A) Grain size distributions for both printing and lateral surfaces of Group-A, Group-B, and Group-C. (B) Grain boundary and microdefects. The observations of the printing and lateral surfaces are consistent; therefore, only the lateral surface features are presented here. Yellow arrows represent the loose grain boundary and blue circles represent microdefects. (C) micro-CT 2D slices and 3D images for Group-A, Group-B, and Group-C.

In experiments evaluating the mechanical properties of ceramics, biaxial flexure is typically used because three- or four-point flexure bars are prone to suffering from defects at their edges, which often initiates fractures.[9] A previous study suggested that polishing can increase flexural strength by eliminating surface defects and that the printing/load orientation can influence flexural strength.[17] To eliminate the effects of these surface factors, the bar specimens in this study were controlled to be printed and loaded with the same orientation, and all surfaces were polished. Especially, the layered structure on the lateral outer surface were removed to avoid the defects. Thus, we assume that the differences in flexural strength (Group-A > Group-B > Group-C) was caused by internal microdefects in the specimen. Y_2O_3 was included in the slurry, so the sintered zirconia is Y_2O_3 particle stabilised zirconia (PSZ) in our article. The load-displacement curve in our study was similar with the PSZ load-displacement curve in the previous articles.[26,27] At ~0.15 mm, the yield starts in our study. Phase transformation from tetragonal to monoclinic during the loading would influence the fracture behavior.[28] This phenomenon is also influenced by the special layered characterisation of 3Dp/ZrO_2. Although the layered structure disappeared in this study after debinding and sintering in 3Dp/ZrO_2 according to SEM and EDS results, we consider that the effects of the layered structure may still be present in the more microscopic structures. Although the flexural strength of Group-B was lower than those of Group-A in both the three-point and biaxial flexure tests, this effect was more evident in the three-point flexure test. Disc specimens have fewer layers and smaller volumes, indicating the interlayer and internal defects of disc specimens are less than bar specimens. Therefore, it is less likely to lead to fractures. In addition, specimen thickness influences their mechanical properties.[16]

In this study, SEM, EDS, and micro-CT were used to investigate the effect of sintering placement orientation on the

mechanical properties of 3Dp/ZrO_2. The SEM image before debinding and sintering clearly showed the layered structure generated during the printing process. In addition, less Zr was observed in the bonding area, indicating a lower distribution of ZrO_2 and higher distribution of resin matrix in this area. Interestingly, we observed a fuzzy transitional boundary at the top of the layer and a clear, straight boundary at the bottom. In a previous study, they observed this structure by analysing the lamellar structure according to the yellowing phenomenon, attributing it to "resin enrichment."[29] It was also reported that ceramic particles sink owing to gravity during layer-by-layer printing, forming an inhomogeneous single cured layer with obvious gaps.[30] Therefore, this phenomenon may result in insufficient density and defect generation in zirconia.

The high-speed sintering group exhibited more small pores at the grain junctions and relatively larger grains and that the high sintering speeds resulted in reduced density.[31] To avoid internal defects and non-compact products, resulting from improper sintering, we applied a slow one-step sintering method according to the manufacturer's instructions. The SEM images of the sintered 3Dp/ZrO_2 revealed that the grain boundaries of Group-B and Group-C were not as tight as those of Group-A. Group-B, which had the lower flexural strength, had more lacuna microdefects with sizes that were approximately the same as those of the smaller grains. We speculate that microdefects and loose grain boundaries are mutually reinforcing. The previous study also observed that defects are often found at grain boundaries, whereas fewer defects allow the grains to be more tightly bonded.[32] During sintering, the resin matrix is removed and ZrO_2 undergoes particle rearrangement and atomic diffusion; thus, the interlayer gap decreases.[30] During this process, 3Dp/ZrO_2 is affected by stress[24], gas expansion pressure[33], interceramic bonding forces[33], and gravity[25]. Gravity and internal stresses promote stronger interlayer bonding when the printing layer orientation is parallel to the horizontal plane during sintering, but not when it is perpendicular. Therefore, the interlayer bonding process was more difficult in the perpendicular sintering placement group than in the parallel sintering placement group.

Although our furnace chamber is relatively small, surrounded by multi-layered refractory insulation and we make efforts to place both the crucible and the specimens at the center of the heating zone, we recognise that small deviations in temperature may still occur due to structural differences within the furnace. Rippe et al.[34] demonstrated that the number and positioning of specimens within the sintering furnace significantly affected the biaxial flexural strength of veneered zirconia, due to uneven heat distribution. Their results showed that specimens placed closer to the resistance device, where heat delivery was more efficient, exhibited up to 2.5 times higher flexural strength than those further away. This highlights the potential impact of thermal gradients within the chamber, even when using standardised sintering protocols. However, in our current study, both the three-point and biaxial flexural strength measurements showed relatively stable values in each group. The standard deviations were 57.10, 102.01, and 38.46 MPa in the three-point test, and 199.37 and 199.71 MPa in the biaxial test. These values suggest acceptable internal consistency and reproducibility of the mechanical properties, supporting the assumption that thermal distribution within our chamber was reasonably uniform under the specific experimental conditions.

Note that cracks (Figure 7A) were observed in some of the bar specimens in Group-C that were not used in three-point flexure test. Figure 7B shows that most cracks were initiated in and extended from the region between the layers, which is consistent with the results of a previous study.[35] It was reported that channels form within the green body during the debinding process to allow decomposition monomers and carbon dioxide to escape, potentially leading to cracking.[22] However, the SEM image of the crack surface (Figure 7B) reveals that the fracture is intergranular (with a clear grain boundary), indicating that the grains first bonded and then fractured. This confirms the incomplete bonding of the grains in Group-C; thus, fracture occurs during the sintering/cooling stage (Figure 7C).

Although ZrO_2 has a wide range of applications, we investigated 3Dp/ZrO_2 using test methods and specimens commonly used in the dental field. Because the shapes of dental prostheses are particularly complex, the anisotropy of 3Dp/ZrO_2 must be adequately investigated for its application in the dental field. In this study, the perpendicular sintering placement orientation resulted in lower mechanical properties and more microdefects. Therefore, it is recommended to maintain the printing layer orientation parallel to the horizontal plane during sintering. Even for printing complex products such as dental crowns, some support objects such as alumina balls should be utilised to control the sintering placement orientation. (Figure 1C)

The anisotropy is related to the shape of the particles, anisotropy will also be retained after sintering owing to the oriented microstructure.[21] Numerous researchers have attempted to use composite particles such as cordierite or ZrO_2 to characterise ceramic printing.[36] The spherical ZrO_2 particles in the slurry in this study were spherical, avoiding any influence on the results owing to their shape. Therefore, complex studies involving different particles and sintering placement orientations could be further analysed. A limitation of this study is that we used a one-step sintering procedure, which made it impossible to analyse the green body. A study analysed the step-by-step decomposition of resin matrix during debinding process by combining the results of the gas products at different debinding temperatures with the thermogravimetric analysis and differential scanning calorimetry results.[22] Moreover, the raw material used in this study was a commercial slurry; thus, the unknown resin matrix hindered the analysis of the debinding process. Two-step sintering and a known resin matrix can be used to further investigate the influence of sintering placement orientation on the mechanical properties and microstructure of 3Dp/ZrO_2.

Furthermore, this study was conducted under in vitro conditions, and the results may be dependent on the specific experimental setup. Finite element analysis (FEA) has been widely used in dentistry and it is demonstrated that material performance can vary significantly based on multiple interacting parameters.[37] Expect material properties, other parameters such as different specimen sizes, specimen structure and loading technique can also influence material performance.[38,39] Therefore, incorporating FEA modeling in future research

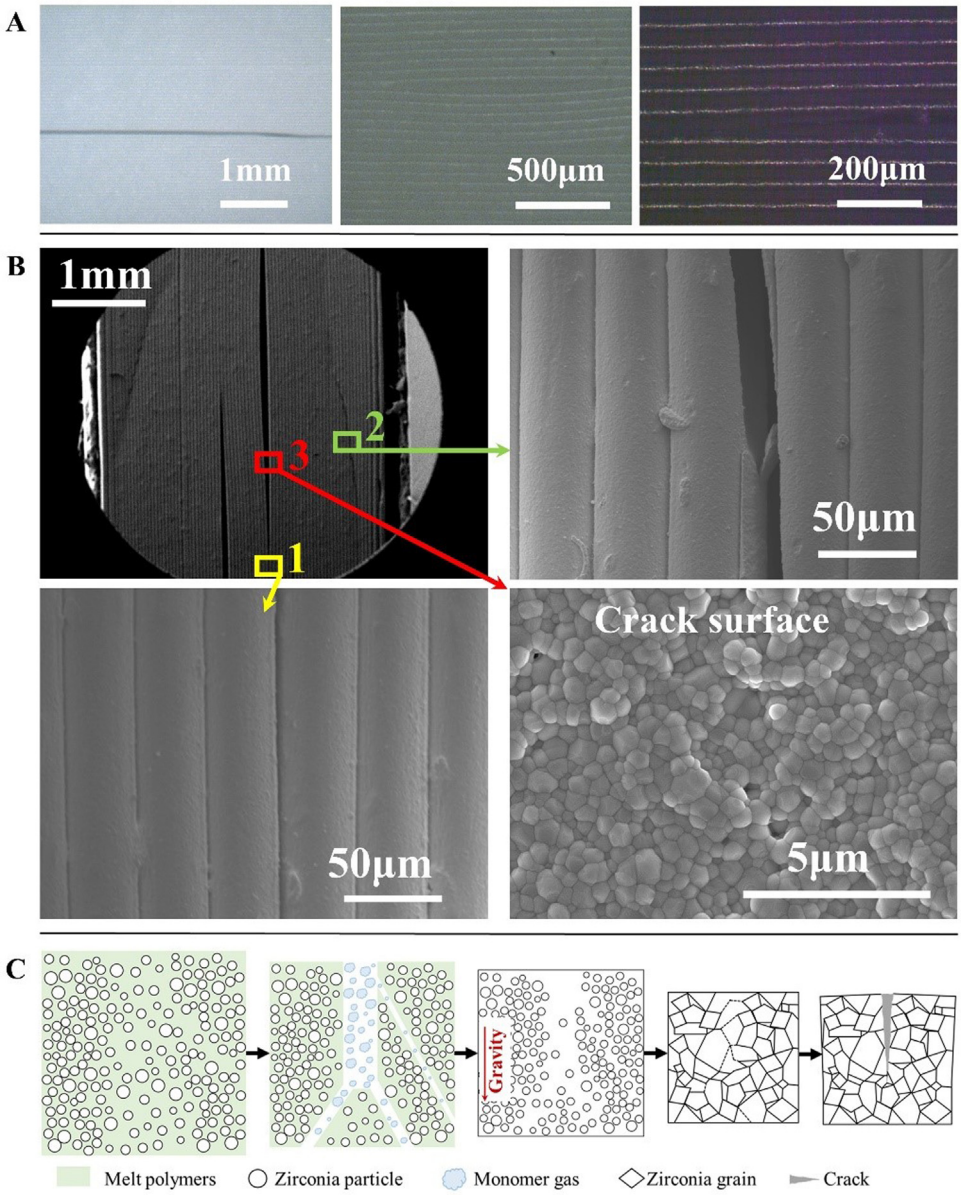

Fig. 7 – (A) Photomicrograph of surface cracks on a sintered 3Dp/ZrO_2 specimen from Group-C. (B) SEM images of the crack, including crack initiation (1: yellow arrow), the crack along the layer structure (2: green arrow), and crack surface grains (3: red arrow). (C) Schematic of the crack process in Group-C. *This specimen was not used for any test. And the layered structure are surface textures resulting from the DLP printing process and are not indicative of internal delamination.

could offer a more comprehensive understanding of stress distributions and mechanical failure modes under different sintering orientations.

Conclusion

This study demonstrate that the sintering orientation significantly influences the mechanical properties and microstructure of 3Dp/ZrO_2. Specimens sintered with printing layer orientation parallel to the horizontal plane exhibited superior flexural strength. Those sintered in perpendicular orientations showed reduced performance, which was attributed to loose grain boundaries and internal microdefects observed in microstructure analysis. These findings present the importance of considering sintering orientation when processing 3Dp/ZrO_2 to ensure the structural reliability and mechanical durability. Also, these findings offer a clear guideline for optimising processing parameters in manufacturing of 3Dp/ZrO_2, and warrant further investigation on complex geometries and clinical restorations.

Author Contributions

Qi Jia: Conceptualisation, Data curation, Formal analysis, Investigation, Software, Visualisation, Writing – original draft;

Seo-Hyun Kim: Data curation, Formal analysis; Yuchuan Xu: Investigation, Formal analysis, Writing – original draft; Chen Ma: Investigation, Formal analysis, Writing – original draft; Kwang-Mahn Kim: Conceptualisation, Writing – review and editing; Heng Bo Jiang: Conceptualisation, Supervision, Validation, Writing – review and editing; Jae-Sung Kwon: Conceptualisation, Funding acquisition, Project administration, Resources, Supervision, Writing – review and editing

Declaration of competing interest

The authors declare that they have no known competing financial interests or personal relationships that could have appeared to influence the work reported in this paper.

Acknowledgements

This work was supported by the Technology Innovation Program (20009652, Technology on commercialisation and materials of Bioabsorbable Hydroxyapatite that is less than micrometer in size) funded By the Ministry of Trade, Industry & Energy (MOTIE, Korea) & the National Research Foundation of Korea (NRF) grant funded by the Korean government (MSIT) (No. 2022R1C1C1010304)

REFERENCES

1. Cesar PF, Miranda RBdP, Santos KF, Scherrer SS, Zhang Y. Recent advances in dental zirconia: 15 years of material and processing evolution. Dent Mater 2024;40(5):824–36. doi: 10.1016/j.dental.2024.02.026.
2. Lin L, Fang Y, Liao Y, Chen G, Gao C, Zhu P. 3D printing and digital processing. Tech Dent 2019;21(6):1801013. doi: 10.1002/adem.201801013.
3. Balhaddad AA, Garcia IM, Mokeem L, et al. Three-dimensional (3D) printing in dental practice: applications, areas of interest, and level of evidence. Clin Oral Investig 2023;27(6):2465–81. doi: 10.1007/s00784-023-04983-7.
4. Alghauli MA, Alqutaibi AY, Wille S, Kern M. The physical-mechanical properties of 3D-printed versus conventional milled zirconia for dental clinical applications: a systematic review with meta-analysis. J Mech Behav Biomed Mater 2024;156(106601). doi: 10.1016/j.jmbbm.2024.106601.
5. Branco AC, Colaço R, Figueiredo-Pina CG, Serro AP. Recent advances on 3D-printed zirconia-based dental materials. Rev J 2023;16(Issue). doi: 10.3390/ma16051860.
6. Su G, Zhang Y, Jin C, et al. 3D printed zirconia used as dental materials: a critical review. J Biol Eng 2023;17(1):78. doi: 10.1186/s13036-023-00396-y.
7. Li X, Zhong H, Zhang J, Duan Y, Li J, Jiang D. Fabrication of zirconia all-ceramic crown via DLP-based stereolithography. Int J Appl Ceramic Technol 2020;17(3):844–53. doi: 10.1111/ijac.13441.
8. Meng J, Lian Q, Xi S, Yi Y, Lu Y, Wu G. Crown fit and dimensional accuracy of zirconia fixed crowns based on the digital light processing technology. Ceramics Int 2022;48(12):17852–63. doi: 10.1016/j.ceramint.2022.03.057.
9. Giugliano TS, Zhang Y, Janal MN, Lim CH, Smith RM, Choi M. In vitro comparison of physical characteristics of milled versus printed zirconia discs. J Prosthodontics 2023 n/a(n/a). doi: 10.1111/jopr.13778.
10. A. Hadian, L. Koch, P. Koberg, et al. Material extrusion based additive manufacturing of large zirconia structures using filaments with ethylene vinyl acetate based binder composition additive manufacturing. 2021;47(102227. https://doi.org/10.1016/j.addma.2021.102227
11. Teegen I-S, Schadte P, Wille S, Adelung R, Siebert L, Kern M. Comparison of properties and cost efficiency of zirconia processed by DIW printing, casting and CAD/CAM-milling. Dent Mater 2023;39(7):669–76. doi: 10.1016/j.dental.2023.05.001.
12. Zenthöfer A, Ilani A, Schmitt C, Rammelsberg P, Hetzler S, Rues S. Biaxial flexural strength of 3D-printed 3Y-TZP zirconia using a novel ceramic printer. Clin Oral Investig 2024;28(2):145. doi: 10.1007/s00784-024-05533-5.
13. Radomski K, Lee Y-H, Lee SJ, Yoon H-I. Effect of exposure energy dose on lateral resolution and flexural strength of three-dimensionally printed dental zirconia. J Adv Prosthodont 2023;15(5):248–58. doi: 10.4047/jap.2023.15.5.248.
14. Liu Y, Liu Y, She W, Cao Y, Zeng Q, Dong N. Effect of reactive diluent concentration on rheological and curing behavior of zirconia ceramic slurry for DLP printing. Int J Appl Ceramic Technol 2024;21(1):62–75. doi: 10.1111/ijac.14493.
15. Liebermann A, Schultheis A, Faber F, Rammelsberg P, Rues S, Schwindling FS. Impact of post printing cleaning methods on geometry, transmission, roughness parameters, and flexural strength of 3D-printed zirconia. Dent Mater 2023;39(7):625–33. doi: 10.1016/j.dental.2023.05.005.
16. Rues S, Herpel C, Ilani A, Schmitt C, Rammelsberg P, Schwindling FS. Effect of firing time and wall thickness on the biaxial flexural strength of 3D-printed zirconia. Dent Mater 2024;40(3):484–92. doi: 10.1016/j.dental.2023.12.018.
17. Lu Y, Wang L, Dal Piva AMO, et al. Influence of surface finishing and printing layer orientation on surface roughness and flexural strength of stereolithography-manufactured dental zirconia. J Mech Behav Biomed Mater 2023;143(105944). doi: 10.1016/j.jmbbm.2023.105944.
18. Xiang D, Xu Y, Bai W, Lin H. Dental zirconia fabricated by stereolithography: accuracy, translucency and mechanical properties in different build orientations. Ceramics Int 2021;47(20):28837–47. doi: 10.1016/j.ceramint.2021.07.044.
19. Lu Y, Wang L, Dal Piva AMdO, et al. Effect of printing layer orientation and polishing on the fatigue strength of 3D-printed dental zirconia. Dent Mater 2024;40(2):190–7. doi: 10.1016/j.dental.2023.11.007.
20. Li H, Liu Y, Liu Y, et al. Evolution of the microstructure and mechanical properties of stereolithography formed alumina cores sintered in vacuum. J Eur Ceramic Soc 2020;40(14):4825–36. doi: 10.1016/j.jeurceramsoc.2019.11.047.
21. Manière C, Kerbart G, Harnois C, Marinel S. Modeling sintering anisotropy in ceramic stereolithography of silica. Acta Materialia 2020;182(163-171). doi: 10.1016/j.actamat.2019.10.032.
22. Wang K, Qiu M, Jiao C, et al. Study on defect-free debinding green body of ceramic formed by DLP technology. Ceramics Int 2020;46(2):2438–46. doi: 10.1016/j.ceramint.2019.09.237.
23. Mascolo MC, Mascolo G, Ring TA. Grain boundary evolution on sintering in yttria (8mol%)-stabilized zirconia assisted by one or two driving forces. J Eur Ceramic Soc 2012;32(16):4129–36. doi: 10.1016/j.jeurceramsoc.2012.07.004.
24. Johansson E, Lidström O, Johansson J, Lyckfeldt O, Adolfsson E. Influence of resin composition on the defect formation in alumina manufactured by Stereolithograph. Materials 2017;10(Issue). doi: 10.3390/ma10020138.
25. Torresani E, German RM, Huff R, Olevsky EA. Influence of gravity on sintering of 3D-printed powder components. J Am Ceramic Soc 2022;105(1):131–46. doi: 10.1111/jace.18056.
26. Wang L, Liu X, Wang G, et al. Partially stabilized zirconia moulds fabricated by stereolithographic additive manufacturing via digital light processing. Mater Sci Eng 2020;770(138537). doi: 10.1016/j.msea.2019.138537.

27. Jang GW, Kim HS, Choe HC, Son Fracture MK. Strength and Mechanism of Dental Ceramic Crown with zirconia thickness. Procedia Eng 2011;10(1556-1560). doi: 10.1016/j.proeng.2011.04.260.
28. Chopra D, Guo T, Gulati K, Ivanovski S. Load, unload and repeat: Understanding the mechanical characteristics of zirconia in dentistry. Dent Mater 2024;40(1):e1–e17. doi: 10.1016/j.dental.2023.10.007.
29. Zhao D, Su H, Hu K, et al. Formation mechanism and controlling strategy of lamellar structure in 3D printed alumina ceramics by digital light processing. Additive Manufacturing 2022;52(102650). doi: 10.1016/j.addma.2022.102650.
30. Zhou S, Zhang S, Zhang C. Fabrication of ZTA crowns with simultaneously improved isotropy on mechanical property and surface quality by DLP international. J Appl Ceramic Technol 2024;21(3):1593–615. doi: 10.1111/ijac.14631.
31. Alshahrani AM, Lim CH, Wolff MS, Janal MN, Zhang Y. Current speed sintering and high-speed sintering protocols compromise the translucency but not strength of yttria-stabilized zirconia. Dent Mater 2024;40(4):664–73. doi: 10.1016/j.dental.2024.02.012.
32. Liu X, Zou B, Xing H, Huang C. The preparation of ZrO2-Al2O3 composite ceramic by SLA-3D printing and sintering processing. Ceramics Int 2020;46(1):937–44. doi: 10.1016/j.ceramint.2019.09.054.
33. Gu Q, Wang H, Gao W, Yu J, Zhou X. Preparation of large-size alumina ceramic parts by DLP 3D printing using high-solid-loading paste and optimizing the debinding process. Ceramics International 2023;49(17, Part B):28801–12. doi: 10.1016/j.ceramint.2023.06.142.
34. Rippe MP, de Melo RM, Moura DMD, et al. The number of specimens in a furnace affects the biaxial flexural strength of veneered zirconia specimens after sintering. J Adhesion Sci Technol 2021;35(6):663–72. doi: 10.1080/01694243.2020.1816790.
35. J. Kim, C. W. Gal, Y.-J. Choi, H. Park, S.-Y. Yoon and H.-s. Yun Effect of non-reactive diluent on defect-free debinding process of 3D printed ceramics. Additive Manufacturing 2023;67 (103475. https://doi.org/10.1016/j.addma.2023.103475
36. Zhang C, Luo Z, Cao J, et al. Mechanical reinforcement of 3D printed cordierite-zirconia composites. Ceramics Int 2022;48 (4):5636–45. doi: 10.1016/j.ceramint.2021.11.108.
37. Celik HK, Koc S, Kustarci A, Rennie AEW. A literature review on the linear elastic material properties assigned in finite element analyses in dental research. Mater Today Commun 2022;30(103087). doi: 10.1016/j.mtcomm.2021.103087.
38. Ismail AM, ElBanna A, Nassef TM, Keilig L, Bourauel C. Is simulation of glued contact sufficient to simulate nonlinear failure behaviour in dental shear bond strength tests? Int Dent J 2025;75(3):1746–58. doi: 10.1016/j.identj.2025.03.007.
39. Kayahan MB, Özkurt-Kayahan Z, Yay K, Kazazoğlu E. 3D FEA of hollow and solid design zirconia dental dowels. J Prosthodont 2016;25(3):229–34. doi: 10.1111/jopr.12289.